Acta Geotechnica (2012) 7:219–237
DOI 10.1007/s11440-011-0157-0

RESEARCH PAPER

Numerical modelling of installation effects for diaphragm walls in sand

Riccardo Conti · Luca de Sanctis · Giulia M. B. Viggiani

Received: 17 June 2011 / Accepted: 19 December 2011 / Published online: 26 January 2012

Abstract The scopes of this work are to study the mechanisms of load transfer and the deformations of the ground during slurry trenching and concreting in dry sand and to evaluate their effects on service structural loads, wall deflections and ground displacements behind the wall caused by subsequent excavation. A series of three-dimensional finite element analyses was carried out modelling the installation of diaphragm walls consisting of panels of different length. The soil was modelled as either linearly elastic-perfectly plastic or incrementally non-linear (hypoplastic) with elastic strain range. Plane strain analyses of diaphragm walls of identical cross section were also carried out in which wall installation was either modelled or the wall was wished in place (WIP). The analyses predict ground movements consistent with the experimental observations both in magnitude and trend. The results also show that the maximum horizontal wall deflections and structural loads reduce with increasing panel aspect ratio towards a minimum which is about twice the value computed for WIP analyses. Panel aspect ratios should be larger than about three to take advantage of the three-dimensional effects. The pattern and magnitude of surface vertical displacements obtained from linearly elastic-perfectly plastic analyses, no matter whether three- or two-dimensional, are unrealistic.

Keywords Constitutive relations · Deformation · Diaphragm and in situ walls · Earth pressure · Numerical modelling and analysis · Sands

List of symbols

B	Excavation width
c'	Shear strength at zero effective stress
E	Young's modulus
e_{c0}	Critical void ratio at zero pressure
e_{d0}	Minimum void ratio at zero pressure
e_{i0}	Maximum void ratio at zero pressure
G	Shear modulus
G_{sec}	Mobilised secant shear modulus
h	Excavation depth
H	Total wall height
h_c	Critical depth
h_s	Granulate hardness
K_0	Coefficient of earth pressure at rest
K_a	Active earth pressure coefficient
K_p	Passive earth pressure coefficient
L	Panel length
M	Bending moment
m_R, m_T	Ratios of characteristic stiffness
N	Axial load in the prop
n	Exponent regulating the decrease of voids ratio with mean effective stress
p'	Mean effective stress
q, q_0	Deviatoric stress and initial deviatoric stress
R	Size of elastic range
t	Panel thickness
u	Horizontal displacement orthogonal to the wall
w	Vertical displacement

R. Conti
SISSA Trieste, Trieste, Italy

L. de Sanctis
Università di Napoli Parthenope, Naples, Italy

G. M. B. Viggiani (✉)
Dipartimento di Ingegneria Civile, Università di Roma Tor Vergata, Via del Politecnico, 1, 00133 Rome, Italy
e-mail: viggiani@uniroma2.it

x	Distance from the centre of the primary panel along the wall
y	Distance from the edge of the trench orthogonal to the wall
z	Depth below ground level
Z	Thickness of sand layer
α, β	Exponents in scalar factors accounting for barotropy and picnotropy
β_R, χ	Exponents regulating transition between different deformation modes
ε_s, ε_{s0}	Shear strain and initial shear strain
ε_v	Volume strain
γ	Soil bulk unit weight
γ_b	Unit weight of bentonite slurry
γ_c	Unit weight of fresh concrete
φ'	Peak friction angle
φ'_c	Critical friction angle
σ'_h	Horizontal effective stress
σ'_v	Vertical effective stress
ψ	Angle of dilatancy

1 Introduction

The construction of underground infrastructures often requires open excavations to be carried out in close vicinity of existing structures. In these conditions, the main design requirement is that of limiting ground deformations caused by excavation. In the last decades, significant advances in the areas of excavation design, construction and analysis have been achieved both for the theoretical and technological aspects; in the field of analysis, the increased availability of commercial computer programs has made the prediction of ground movements using numerical analyses more widespread.

Despite the fact that the finite element method permits to model the whole sequence of operations occurring during construction of deep excavations, the installation of diaphragm walls is still often ignored in the analyses, although it is now widely accepted that the effects associated with slurry trenching and concreting can cause significant displacements of the surrounding ground, of the same order of magnitude as those caused by subsequent excavation in front of the wall, and influence the behaviour of the retaining structure during the main excavation stage. Published data show that the maximum settlement connected to wall installation can reach values of up to 0.15% and extend to a distance of up to twice the maximum depth of the trench [5].

Most past work on installation effects, including full scale monitoring of structures [21, 40] centrifuge testing [2, 35] and numerical modelling [14, 15, 24, 34], has concentrated on the case of heavily overconsolidated deposits, where the in situ horizontal effective stress is generally larger than the vertical effective stress. In these conditions, wall installation tends to reduce the lateral effective stress in the soil near the wall [21, 40], causing substantial ground movements towards the trench that add to those associated with the main excavation stage. Moreover, if installation is not modelled, computed values of prop forces and bending moments are quite high, as, in the analyses, high lateral pressures on the retained side of the wall persist after excavation in front of the wall, that is, the pressure behind the wall does not reach its active value [32]. As installation reduces the applied stresses on the retained side, it reduces prop or anchor forces, and bending moments as both observed in the field [41] and obtained by numerical analyses [15, 16].

Only relatively recently has the case of coarse-grained deposits or soft clays, with low values of the coefficient of earth pressure at rest, been examined [23, 36, 37]. This time, the variation of the state of stress induced in the ground during wall installation might correspond to an increase of the initial horizontal stress at the boundary of the trench, from its in situ value to the hydrostatic pressure of the bentonite slurry, and then to a value approximating to the hydrostatic pressure of the wet concrete, at least in the upper 5–10 m of the wall [10, 15]. During this process, the faces of the trench will deform outwards and it is likely that some heave will be induced in the surrounding ground, before the main excavation stage. As a matter of fact, outwards displacements of the surrounding ground and small amounts of surface heave have been recorded during the concreting stages of diaphragm walls in soft clay [10, 20] and sand [42]. The increase of the state of horizontal stress on the retained side, towards a value that is closer to the passive condition, should also cause an increase in the final values of excavation induced settlements, wall deflections and service structural loads.

Plane strain numerical analyses of installation of diaphragm walls are not realistic as, during the excavation of panels of finite length supported by slurry and the subsequent phases of placing and hardening of concrete, three-dimensional effects can be very significant both for stress transfer and ground deformation. Modelling the installation of a diaphragm wall in plane strain overpredicts the magnitude of soil displacements and the degree and extent of horizontal stress change [8, 15, 25, 34]. Three-dimensional modelling of wall installation [14, 36] and carefully instrumented case histories [30] has shown that the magnitude of displacements and stress changes around the trench depend strongly on panel dimensions.

The scope of this paper is to study the mechanisms of load transfer and the deformations of the ground during slurry trenching and concreting in sand and to evaluate

their effects on service structural loads, wall deflections and ground displacements behind the wall caused by subsequent excavation. The problem examined refers to an ideal case, which permits to isolate the effect of modelling the installation stage and of some constitutive assumptions from the many other factors playing a major role in the successful prediction of the performance of real excavations.

A series of three-dimensional finite element analyses were carried out, modelling the installation and the subsequent behaviour of diaphragm walls consisting of panels of different length, supported by one prop at the top, in a layer of medium dense dry sand. The soil was modelled as either linear elastic perfectly plastic with Mohr–Coulomb failure criterion or using an incrementally non-linear hypoplastic model with elastic strain range [27]. For comparison, plane strain analyses were also carried out in which the wall was wished in place (WIP).

2 Finite element analyses

A series of numerical analyses of a long rectangular excavation of width $B = 12$ m and depth $h = 5$ or 10 m, in a layer of medium dense dry sand with a unit weight $\gamma = 18$ kN/m^3 and a thickness $Z = 18$ m, were carried out (see Fig. 1). The excavation was retained by concrete diaphragm walls with one level of support at the top, of total height $H = 7$ or 13 m, and thickness $t = 0.5$ or 0.7 m, respectively. The diaphragm walls were either WIP or their installation explicitly modelled (WIM) in three-dimensional analyses of slurry trenching and concreting of panels of different length $L = 1$, 2.5, and 4 m, or in plane strain ($L \rightarrow \infty$).

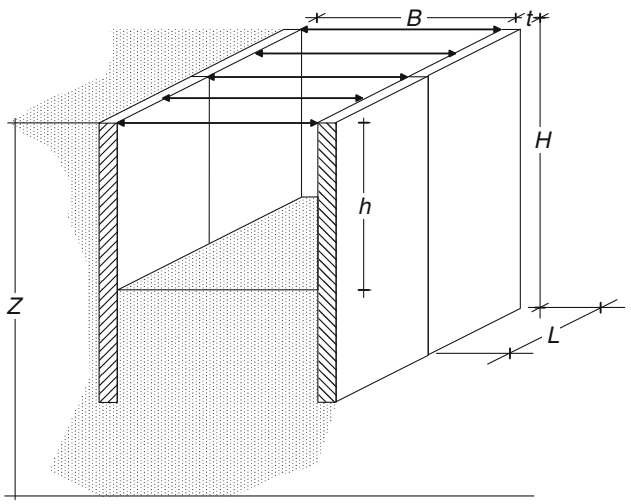

Fig. 1 Problem geometry

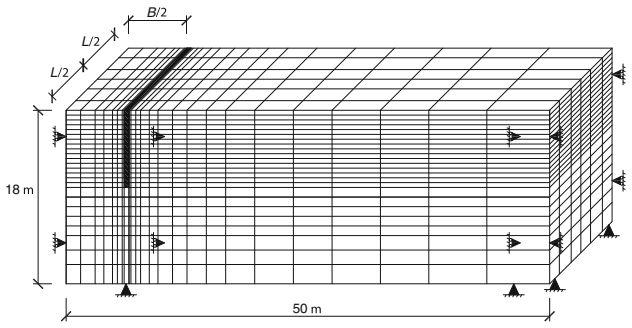

Fig. 2 Three-dimensional finite element mesh

Figure 2 shows the typical three-dimensional finite element mesh used in the study, consisting of 20-node quadratic brick elements. The mesh is 50 m wide and has a variable length equal to the dimension of one panel, L. The base of the mesh is fixed so as to prevent displacements in all directions. The displacements of all vertical boundaries of the mesh normal to the boundary are set to zero. The left-hand boundary corresponds to the plane of symmetry along the centre line of the excavation at a distance $B/2$ from the wall; the right-hand vertical boundary is at a distance from the wall of more than three times its total height, H, and is considered sufficiently remote not to influence wall behaviour. The mesh includes only two half panels. As the lateral boundaries of the mesh also correspond to planes of symmetry, installation of half the first panel corresponds to simultaneous installation of all odd panels, while installation of half the adjacent panel corresponds to simultaneous placement of all even panels.

For the plane strain analyses, a two-dimensional mesh consisting of 8-node biquadratic elements, identical in cross section to the three-dimensional mesh shown in Fig. 2, was used.

2.1 Constitutive models and material properties

One of the most important idealisations in the numerical analysis of boundary value problems is the choice of an appropriate constitutive model for the soil, which, in principle, should be able to reproduce the main features of soil behaviour such as irreversibility, non-linearity and stress-history dependence. Numerical analyses in which linear elastic plastic behaviour is assumed generally fail to predict the observed pattern of ground movements around excavations [3]. Although relatively simple and easy to implement, non-linear elastic plastic formulations (see e.g. [18, 38]) suffer from a number of shortcomings (see e.g. [33]). An alternative to variable moduli elastic plastic models is to adopt generalised plasticity formulations capable to reproduce the observed incremental non-linearity even for stress states well inside a bounding surface

Table 1 Parameters of the hypoplastic model for Hoechstetten sand

φ_c (°)	h_s (MPa)	n	e_{d0}	e_{c0}	e_{i0}	α	β	R	m_R	m_T	β_R	χ
33	1,500	0.28	0.55	0.95	1.05	0.25	1	1×10^{-4}	5	2	1	6

[29]; for this purpose, many models have been proposed to date within the framework of bounding surface plasticity (e.g. [6, 7]) or kinematic hardening plasticity (e.g. [1, 39]).

A completely different approach is followed by hypoplastic, or incrementally non-linear, constitutive models (see e.g. [19]), in which there is a continuously non-linear dependence of the tangent stiffness tensor on the strain rate direction. Unlike incrementally non-linear plasticity theories, in hypoplastic formulations, a non-linear and irreversible response is obtained without the need of a decomposition of the strain tensor. Hypoplastic models have been shown to perform very well for deformations on monotonic loading paths; however, application to small amplitude stress or strain cycles revealed some defects, connected to the inability to reproduce the observed high stiffness on stress reversals and the excessive accumulation of deformation predicted for small amplitude stress cycles.

An extension of a hypoplastic model for cohesionless soils originally developed by von Wolffersdorff [44] was proposed by Niemunis and Herle [27] to include an elastic strain range. In this model, the high stiffness of the soil on changes of the strain path is dealt with by an additional tensorial state variable, called intergranular strain, representing the deformation of the interface layer between the grains. The elastic region is formulated in strain space, and stiffness depends on rotations of the strain path; on total strain path reversal, the soil exhibits a quasi-elastic stiffness within a small-strain range of the order of 10^{-2}%.

The original model by von Wolffersdorff [44] requires eight material parameters independent of stress state and relative density, namely: (1) the critical friction angle, φ_c, (2) the granulate hardness, h_s, with the dimension of stress, used as a reference pressure, (3) the exponent n, regulating the decrease of the minimum, critical and maximum void ratio with increasing mean effective stress from their values at zero pressure, (4) e_{d0}, (5) e_{c0}, and (6) e_{i0}, and two exponents (7) α and (8) β, which appear in the two scalar factors that take into account the dependence of material behaviour on mean effective stress and voids ratio, respectively.

Five additional constants are required for the small-strain extension of the model, of which three, that is, the size of the elastic range, R, and two ratios of characteristic stiffnesses, m_R and m_T, have a clear physical meaning and two, β_R and χ, are exponents related to the transition between different deformation modes (intergranular strain and grain rearrangement). The complete set of parameters for the hypoplastic model, obtained by Niemunis and Herle [27] for medium dense Hoechstetten sand, is given in Table 1. A small shear strength at zero effective stress, $c' = 5$ kPa, was also specified since, if a value of zero is used, a limit state condition would occur at the soil surface, causing numerical difficulties; this was obtained adding to the components of the stress tensor σ'_{ij} a constant value ($=c'/\tan\ \varphi' \cdot \delta_{ij}$). The reader is referred to Niemunis and Herle [27] for the constitutive equations and to Herle and Gudehus [17] for the experimental procedures to determine the values of the parameters.

For comparison, the same problem was also analysed modelling the soil as an isotropic linear elastic perfectly plastic material with Mohr–Coulomb failure envelope and non-associated flow rule ($\psi = 0$). As the mathematical structure and the physical meaning of the relevant parameters of the two constitutive models are different, the problem arises of the selection of appropriate parameters to render the comparison meaningful. In this case, the hypoplastic predictions of material behaviour were considered as the reference to calibrate the parameters of the simpler Mohr–Coulomb model. These were obtained fitting the response of the hypoplastic model in numerical drained triaxial compression tests at increasing confining pressures, yielding a peak friction angle, $\varphi' = 35°$ and a cohesion, $c' = 9$ kPa. The shear stiffness, G, of the Mohr–Coulomb model was taken to increase linearly with depth, from 1 MPa at surface to 8 MPa at mid-height in the sand layer. This corresponds to a shear modulus that is about 20% of the small-strain shear modulus of the hypoplastic model, or a shear strain level of about 0.4%, characteristic of the expected level of deformation during the main excavation stage [2].

The hardened concrete was always modelled as linear elastic, with Young's modulus, $E = 31.2$ GPa, and perfect contact was assumed between the soil and the wall. The analyses carried out using the Mohr–Coulomb model were repeated using interface elements at the contact between the wall and the soil with reduced values of the strength parameters, as detailed in the following.

2.2 Sequence of construction stages

The in situ stress state was prescribed in terms of the earth pressure coefficient at rest $\sigma'_h/\sigma'_v = K_0\ (=1 - \sin\ \varphi')$. Wall construction started with the excavation of the primary

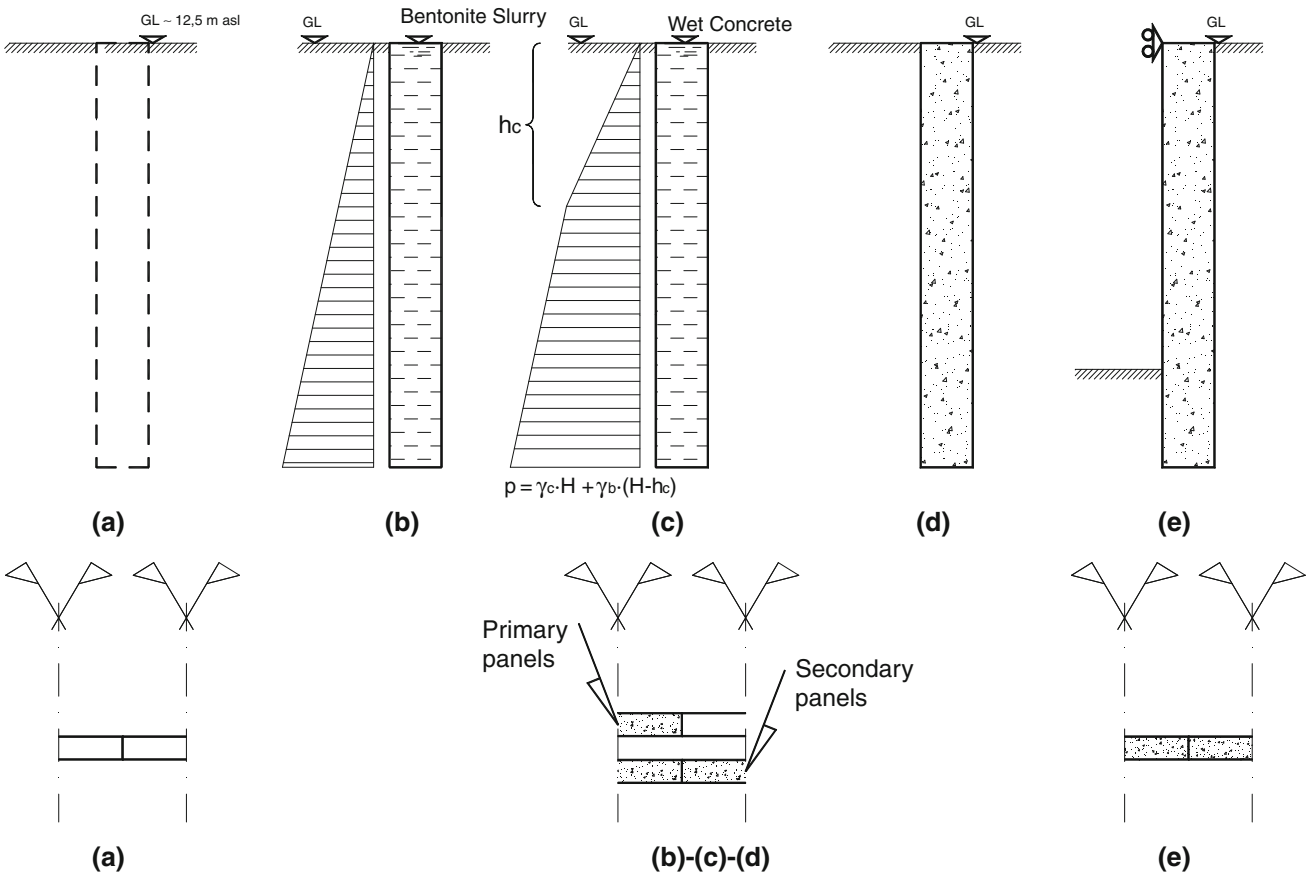

Fig. 3 Sequence of construction stages: **a** in situ stress, **b** slurry trenching, **c** concreting, **d** hardening of concrete and **e** excavation in front of the wall

panel under bentonite slurry, followed by placement of wet concrete and subsequent hardening (Fig. 3). The adjacent secondary panel was then constructed with the same procedure. This sequence of construction stages closely models construction of the diaphragm wall by alternate placement of primary and secondary panels if installation effects do not extend significantly beyond a distance of one panel length; this issue is discussed further in the following.

The excavation of each panel is modelled by removing the soil elements corresponding to the panel and applying to the exposed element faces the hydrostatic pressure of the bentonite slurry acting in the trench. The applied nodal loads correspond to a bentonite slurry with a unit weight $\gamma_b = 11$ kN/m^3. Additional loads are then applied, to model a bilinear distribution of wet concrete pressure in which full hydrostatic pressure of concrete only acts above a critical depth $h_c = 5$ m [22], while below this depth the lateral pressure exerted by wet concrete is taken to be $\gamma_c h_c + \gamma_b(z - h_c)$, in which $\gamma_c = 23$ kN/m^3 is the unit weight of fresh concrete. The nodal loads are then removed and linear elastic elements, representing the hardened concrete panel, are activated in the trench. Finally, the horizontal displacements of the node at the top of the wall are restrained, to simulate an incompressible prop, and the main excavation in front of the wall is carried out, removing the soil in front of the wall in five consecutive steps (Fig. 3e).

The results of the analyses are presented in terms of computed stress changes at various positions around the trench, and ground movements during wall installation, wall deflections, surface settlements behind the wall, bending moments and prop forces during the main excavation stage. Unless otherwise stated, the presented results are those obtained using the hypoplastic model.

3 Wall installation

Figure 4 shows the profiles of horizontal stress computed modelling wall installation in plane strain (WIM 2D), at distances of 0.1 and 3.75 m from the excavation, for $H = 7$ m.

At the boundary of the trench (0.1 m), the horizontal stresses increase from their original at-rest value both during the bentonite stage and the concreting stage, while they fall below their original value immediately beneath

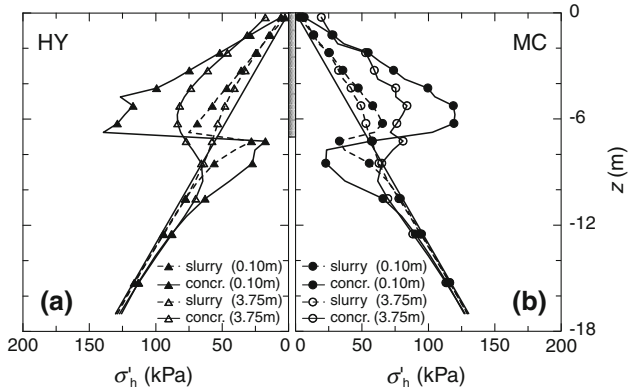

Fig. 4 WIM 2D analyses, $H = 7$ m. Computed horizontal stress during wall installation at 0.1 and 3.75 m from the trench, using: **a** hypoplastic and **b** Mohr–Coulomb model

the bottom of the trench, owing to the restraint provided by the underlying soil. Changes in the horizontal stress are apparent also at some distance away from its boundary (3.75 m), although they become less significant moving away from the trench. The stress distributions obtained using the two constitutive models are very similar, as expected in a stress-controlled problem.

Figure 5 shows the profiles of horizontal stress during installation of the wall with $H = 7$ m, and panel length $L = 2.5$ m, at a distance of 0.1 m from the trench, at the centre and near the edge of the primary and of the secondary panels.

After installation of the primary panel, the horizontal stresses over the depth of the trench increase in the centre and near the edge of the primary panel, while they decrease near the edge and in the centre of the secondary panel. Due to lateral stress transfer, the reduction of the horizontal stresses below the bottom of the trench is less pronounced than in the plane strain analyses, and the horizontal stresses recover their original values more rapidly with depth.

The horizontal stresses behind the centre and near the edge of the primary panel reduce after installation of the secondary panel; simultaneously, the horizontal stresses behind the centre and near the edge of the secondary panel increase to similar values as those attained behind the primary panel during installation of the primary panel. At the end of installation, the horizontal stresses behind the centre of the secondary panel are very similar to those obtained with the WIM 2D analyses. However, the horizontal stresses behind the primary panel are smaller than those obtained by WIM 2D analyses, particularly near the edge where they return more or less to their at-rest values.

The results obtained for $H = 13$ m are qualitatively very similar to those presented in Figs. 4 and 5 for the shorter panels and are not discussed for brevity.

In Fig. 6, the horizontal stresses at a distance of 0.45 m from panels with height $H = 7$ m and different lengths

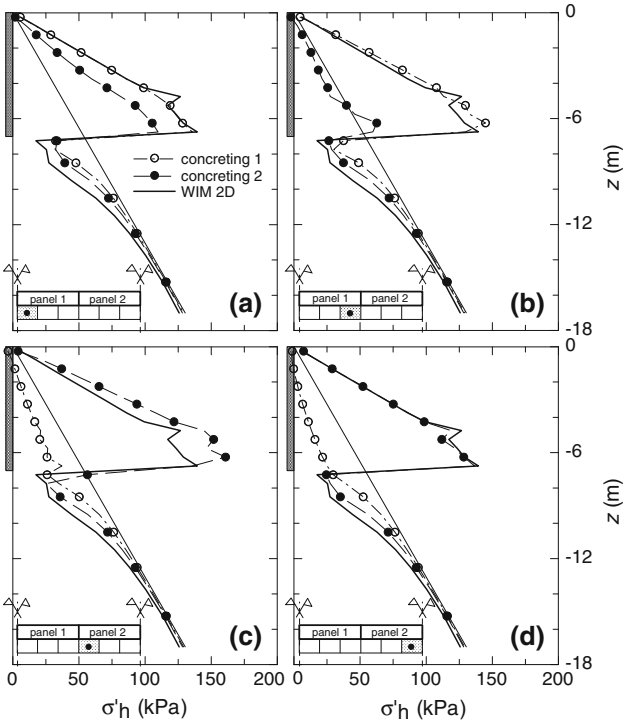

Fig. 5 WIM 3D analyses, $H = 7$ m, $L = 2.5$ m. Computed horizontal stresses during wall installation at 0.1 m from the trench at: **a** centre and **b** near the edge of *panel 1*, **c** near the edge and **d** centre of *panel 2*

L (=1, 2.5, 4 m) on a horizontal section at about mid-height of the wall are plotted with distance from the centre of the primary panel normalised by the length of the panels, x/L. After installation of the primary panel, for longer panels ($L = 2.5$ and 4 m), the horizontal stress in the centre of the primary panel reaches the same value as that predicted by the plane strain analyses ($L \to \infty$), while for the shorter panel, with $L = 1$ m, the horizontal stress fails to reach the plane strain value, due to stress transfer around the trench. At the end of the installation process, the horizontal stress behind the primary panel are always significantly lower than those computed in plane strain; for shorter panels, where three-dimensional effects are more pronounced, also the stresses behind the secondary panel are smaller than those computed in plane strain.

The effects of installation on the initial stress conditions extend beyond the distance of half panel length from the edge of the trench. This is not entirely consistent with previous results obtained for clays both stiff [14, 26] and soft [36] showing that the horizontal stress returns to the initial magnitude within between about one third and half one panel length.

Figure 7 shows the profiles of the horizontal displacements of the excavation boundary and of the vertical displacements at surface calculated in the two-dimensional analyses, immediately after excavation of the trench under

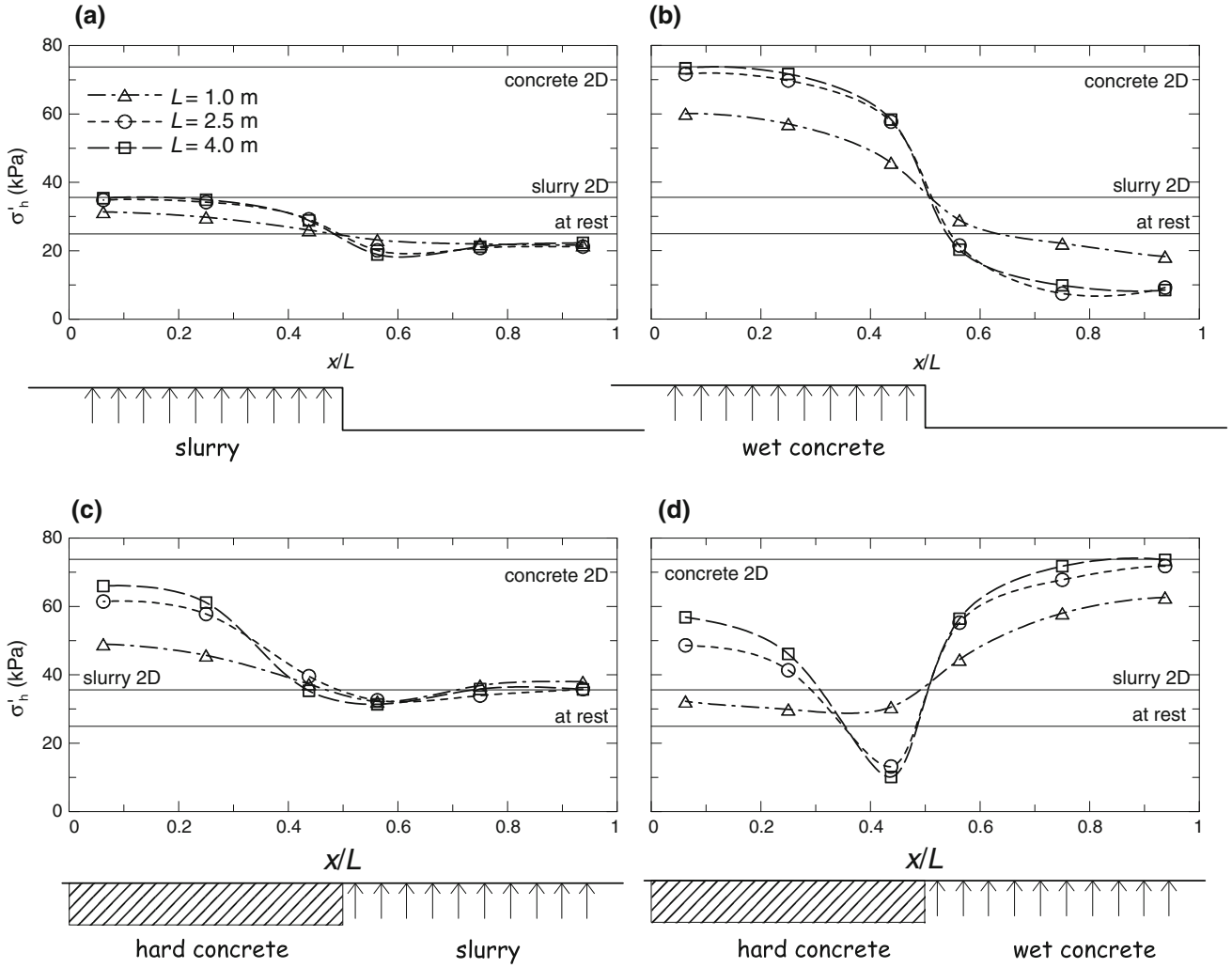

Fig. 6 WIM analyses, $H = 7$ m. Distribution of horizontal stresses along panels of different length and in plane strain at a distance of 0.45 m from the trench and about mid-height of the wall ($z = -3.25$ m): **a** slurry trenching of *primary panel*, **b** concreting of *primary panel*, **c** slurry trenching of *secondary panel* and **d** concreting of *secondary panel*

the bentonite support slurry and immediately after concreting, for $H = 7$ m. Once again, the results obtained for $H = 13$ m are qualitatively very similar to those for the shorter panels and are not shown for brevity.

Outwards displacements and heave of the ground surface are computed both for slurry trenching and concreting, with the magnitude of ground displacements reducing rapidly below the toe of the wall and with increasing distance from the trench, due to non-linearity of soil behaviour. At ground surface, vertical displacements extinguish at a distance of about $2.5 \times H$.

The trend of the horizontal displacements obtained using the simpler Mohr–Coulomb model is similar to that computed using the hypoplastic model; however, the maximum horizontal displacement occurs at a shallower depth, and the horizontal displacements extend slightly deeper below the toe of the wall. The displacements computed using the Mohr–Coulomb model are much larger than using the hypoplastic model; in particular, unrealistic heave of the ground surface is obtained, about 5 times that computed using the hypoplastic model, and closer to the boundary of the trench. This result is partly due to the fact that the secant elastic modulus of the Mohr–Coulomb model was evaluated at the expected strain level during the main excavation stage, which is larger than the average deformation mobilised in the soil surrounding the trench during installation.

Figure 8 shows the profiles of maximum horizontal displacements and of vertical displacements at surface with distance from the boundary of the trench, all normalised by the depth of the trench, H. To predict the same maximum horizontal displacement at the border of the trench as from the hypoplastic analyses, the stiffness of the Mohr–Coulomb model had to be increased to about twice the original

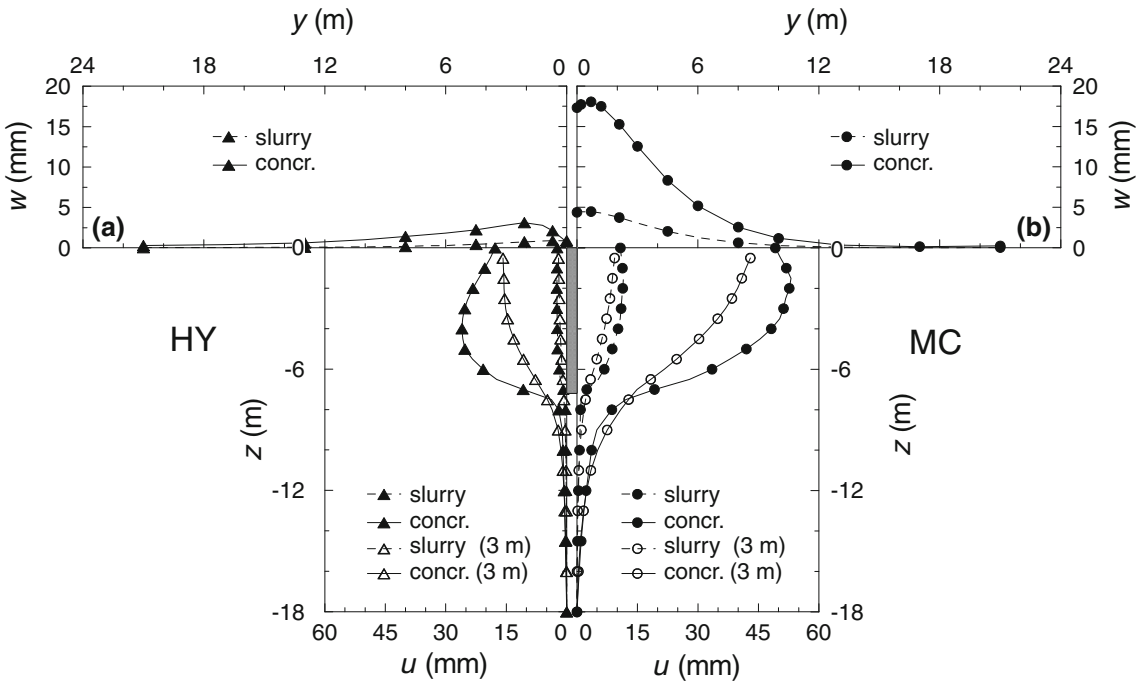

Fig. 7 WIM 2D analyses, $H = 7$ m. Distribution of horizontal displacements at the border of the trench and 3 m away from the trench and settlements of ground surface computed during installation with: **a** hypoplastic and **b** Mohr–Coulomb model

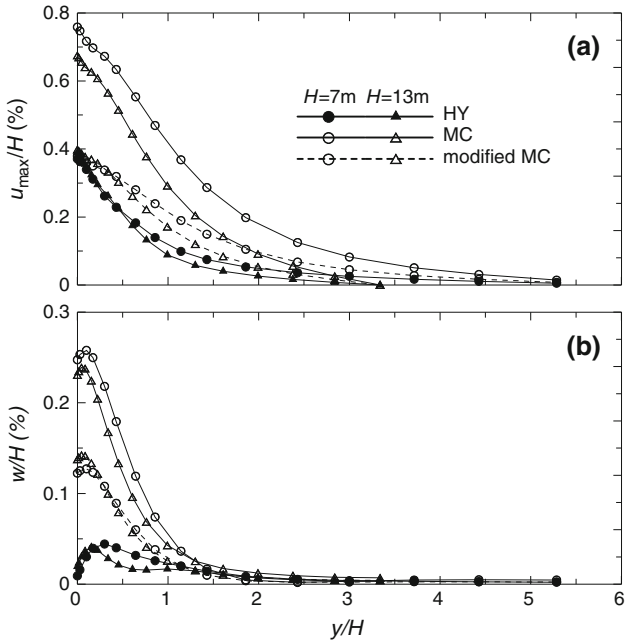

Fig. 8 WIM 2D analyses. Profiles of: **a** maximum horizontal displacement and **b** vertical displacement at surface, with distance from the boundary of the trench, all normalised by the depth of the trench, H

one, approximately corresponding to the deformation level mobilised in the installation stage ($\cong 0.2\%$). Still, the reduction of the maximum horizontal displacement with distance from the trench cannot be predicted correctly. Also, the maximum computed heave is reduced, but it is still about three times that computed using the hypoplastic model.

Figure 9 shows the horizontal displacements along the excavation boundary and the surface vertical displacements at the centre of the primary panel, at the contact between the two panels, and at the centre of the secondary panel, at the end of the installation of primary and secondary panels ($H = 7$ m, $L = 2.5$ m).

The horizontal displacements of the primary panel and at the contact between the two panels develop during installation of the primary panel. No further horizontal displacements of the primary panel once cast are experienced during installation of the secondary panel, while the displacements of the secondary panel increase reaching final values that are larger than those at the centre of the primary panel. This leads to a non-uniform horizontal displacement profile along the length of the wall (Fig. 10). The horizontal displacements of the boundary of the trench computed in the plane strain analyses are much larger than those computed from the 3D analyses, due to the restraint provided by the surrounding ground.

The profiles of vertical displacements at ground surface show that, at the end of installation, at all positions, the outwards movements of the boundary of the excavation are accompanied by settlements near the trench and small heave away from the trench. The corresponding Mohr–Coulomb analyses predict surface heave at all positions.

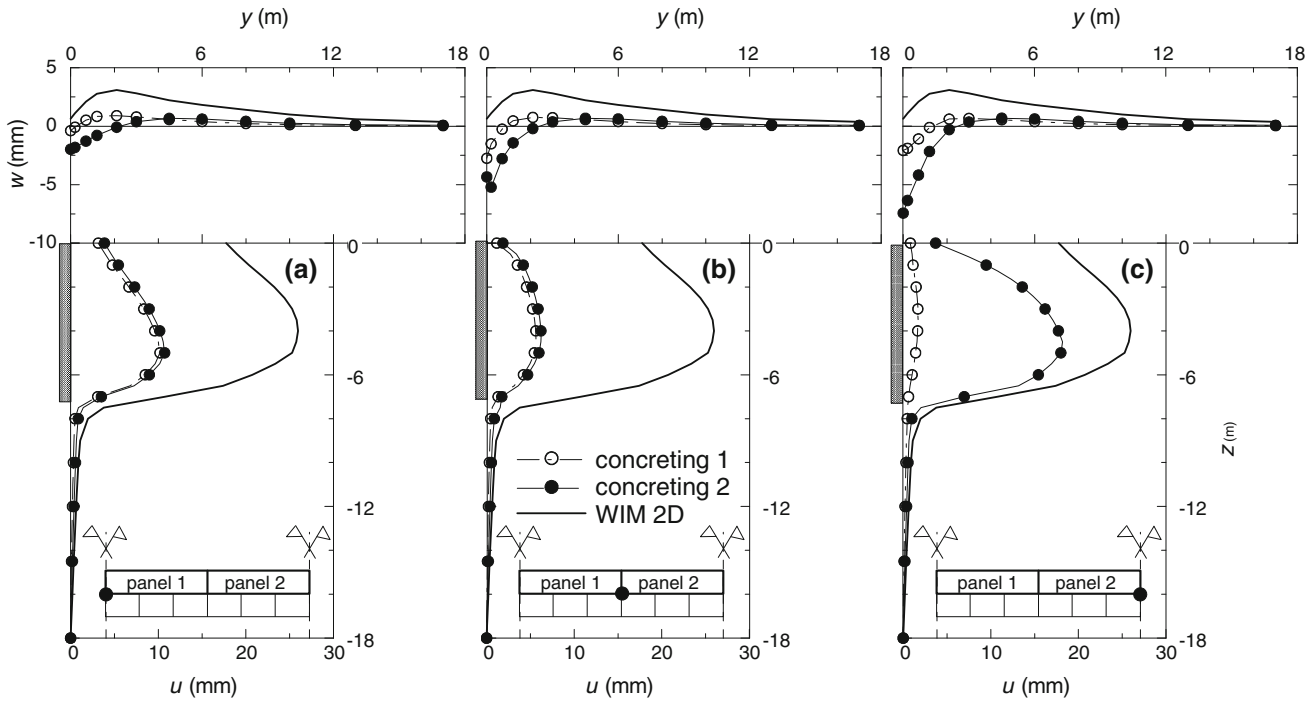

Fig. 9 WIM 3D analyses. Horizontal displacements along the excavation boundary and vertical displacements of the surface at: **a** centre of *panel 1*, **b** contact of the *two panels* and **c** centre of *panel 2*

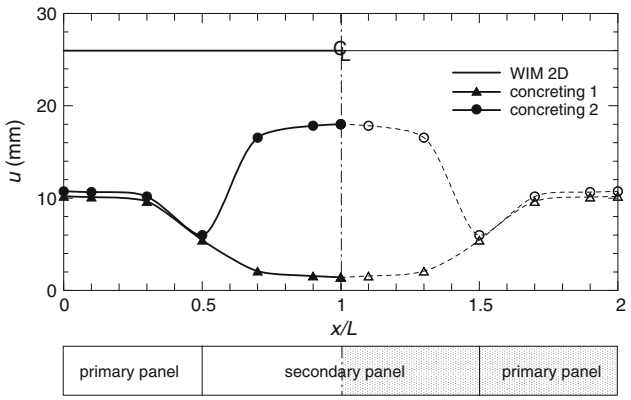

Fig. 10 WIM 3D analyses, $H = 7$ m, $L = 2.5$. Maximum horizontal displacement profiles at the end of the installation of the *primary* and of the *secondary panel*

Figure 11 shows the final profiles of the horizontal displacements of the excavation boundary and of the vertical displacements of the ground surface, for $H = 7$ m and for a range of panel lengths L (=1, 2.5, 4 m) and in plane strain ($L \rightarrow \infty$). The maximum outward horizontal displacement increases with increasing panel length, moving towards the value computed from plane strain analyses. The results of the three-dimensional analyses indicate that near the trench, at all positions, the ground settles by an amount that increases with panel length. The same figure shows the results obtained for two analyses carried out for unrealistically long panels ($L = 12$ and 18 m). This time, the horizontal displacements at the centre of the secondary panel exceed those computed in plane strain. This is due to the fact that, while for the primary panel the conditions immediately before installation are the same as for 2D analyses, the conditions around the secondary panel before installation have been altered by construction of the primary panel.

Figure 12 shows the final profile of horizontal displacements along the length of the wall at a depth of 5 m, for $H = 7$ m and different lengths L (=1, 2.5, 4, 12 and 18 m) and in plane strain ($L \rightarrow \infty$). The maximum horizontal displacement at all locations increases as the length of the panel is increased. Only with unrealistic values of panel length ($L = 12$ and 18 m), the profiles of horizontal displacements along the primary panel become closer to one another and to the plane strain values.

Figure 13 shows the maximum horizontal displacements at the centre of the primary and of the secondary panel, normalised by the corresponding displacement calculated in the plane strain analyses, as a function of the panel depth-to-length ratio, H/L. As the panel aspect ratio, H/L, is reduced, the maximum horizontal displacements increase at an accelerating rate; consistently with the results obtained by Gourvenec and Powrie [14], the curves suggest that the panel aspect ratios, H/L, should be larger than about three to take advantage of three-dimensional effects to minimise ground movements.

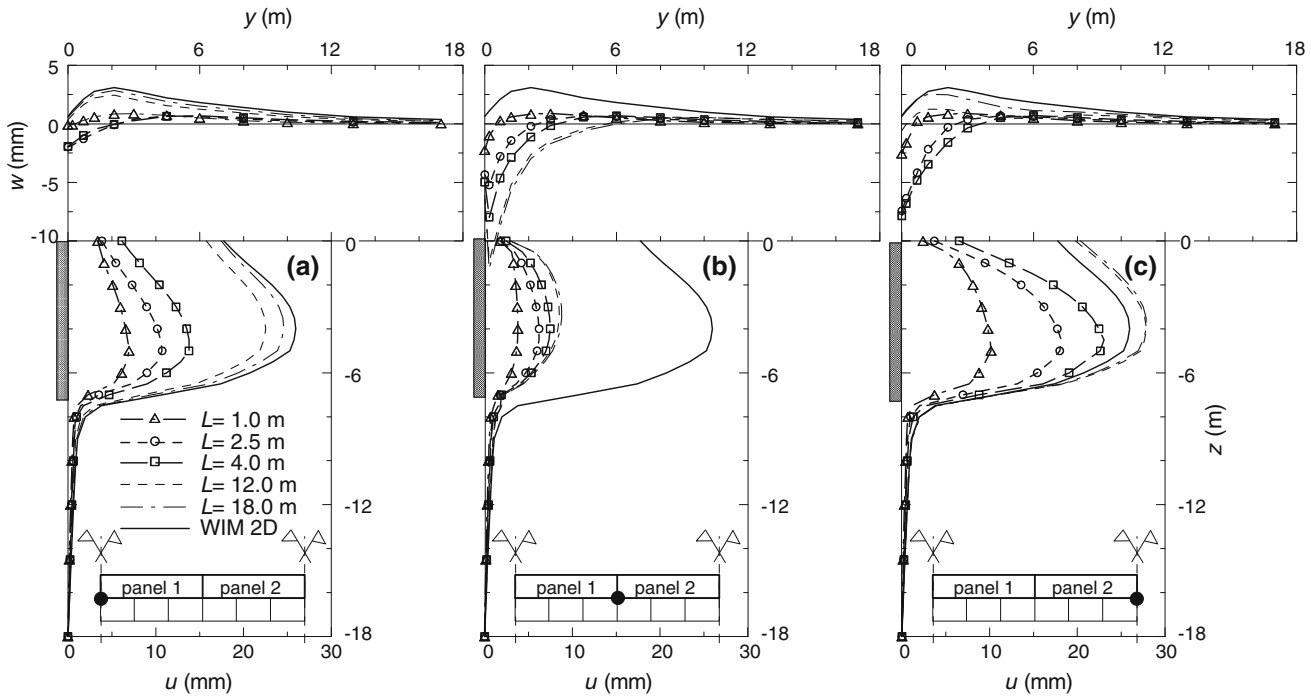

Fig. 11 WIM analyses, $H = 7$ m. Distribution of final horizontal displacements at the border of the trench and vertical displacements of ground surface for panels of different lengths and in plane strain at: **a** centre of *panel 1*, **b** contact of the *two panels* and c centre of *panel 2*

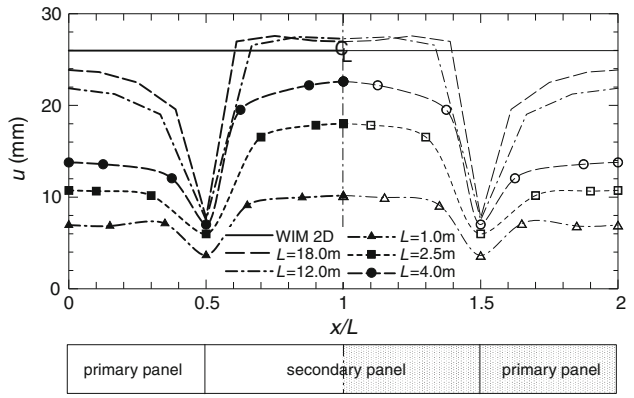

Fig. 12 WIM analyses, $H = 7$ m. Profiles of final horizontal displacements at a depth of 5 m, along *panels* of different lengths and in plane strain

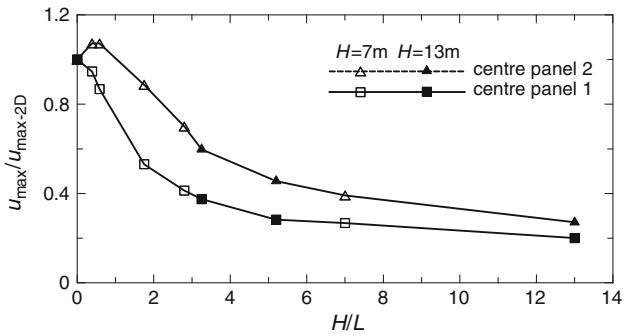

Fig. 13 Maximum horizontal displacements at the centre of the *primary* and of the *secondary panel* normalised by the corresponding plane strain displacements as a function of panel aspect ratio, *H/L*

3.1 Comparison with a realistic sequence of panel installation

An oscillating distribution of horizontal stress behind primary and secondary panels is obtained also from numerical analyses in which a more realistic sequence of panel installation is modelled. Figure 14 shows the distribution of horizontal stress on a horizontal section at $z = -3.5$ m and a distance $y = 0.4$ m from the wall at the end of the installation of four panels with height $H = 13$ m and length $L = 2.5$ m in an alternate sequence (1–2–3–4), together with the distribution obtained simulating the installation of only two half panels of the same dimensions in double symmetry, as described above. The difference of computed horizontal stress behind the secondary panel is only about 8%, confirming that the simplified approach adopted in this study yields realistic predictions of horizontal stress distributions, both qualitatively and quantitatively, despite the fact that installation effects extend further than half panel length from the edge of the trench. Also the horizontal displacements computed simulating the installation of four panels compare well with those obtained simulating the installation of only two half panels in double symmetry (Fig. 15). In this case, the maximum difference in the computed horizontal displacements behind the secondary

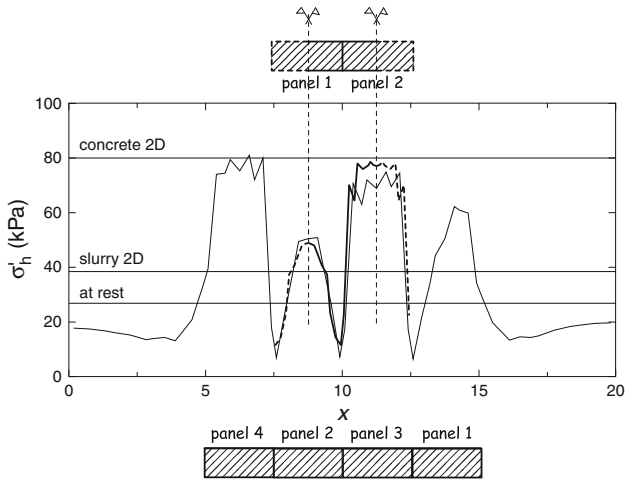

Fig. 14 WIM 3D analyses, $H = 13$ m, $L = 2.5$ m. Distribution of horizontal stress at a distance $y = 0.4$ m from the wall on a horizontal section at $z = -3.5$ m at the end of the installation of *four panels* or *two half panels* in double symmetry

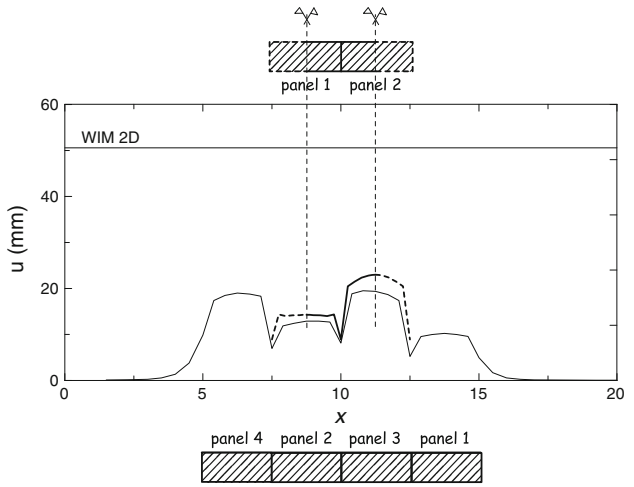

Fig. 15 WIM 3D analyses, $H = 13$ m, $L = 2.5$ m. Distribution of horizontal displacements at the boundary of the trench on a horizontal section at $z = -5$ m at the end of the installation of *four panels* or *two half panels* in double symmetry

panel is about 16%, which is slightly larger than for horizontal stress but, in our opinion, still acceptable.

4 Excavation

4.1 Evaluation of model performance

One of the main effects of wall installation is the significant change in the in situ stresses before the main excavation stage. For all wall lengths, both behind primary and secondary panels, wall installation tends to increase the initial lateral effective stress in the soil near the wall, causing the resulting stress state to be larger than the at-rest condition; on the other hand, near the edge of the panels, the horizontal effective stress is locally close to its active value, particularly for longer panels (see Fig. 6d).

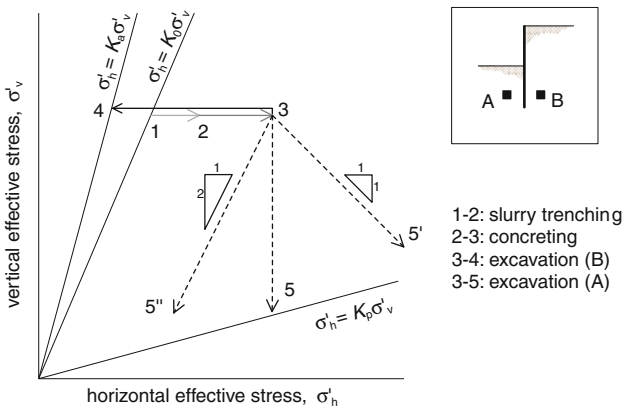

Fig. 16 Typical effective stress paths for soil elements behind and in front of retaining wall

A second effect concerns the soil stiffness during excavation and its dependence on the direction of the effective stress path in relation to the recent stress history [31, 39]. Figure 16 shows typical effective stress paths for points such as A and B located below dredge line on the excavated and the retained sides of the wall, respectively. At both positions, wall installation should correspond to an increase of horizontal effective stress at approximately constant vertical effective stress. In the subsequent excavation stage, for a smooth wall, a point such as B should experience a reduction of horizontal effective stress at approximately constant vertical effective stress, moving towards active failure. On the other hand, for a soil element such as A, while the vertical effective stress is reduced during excavation, the associated change in the horizontal effective stress results from the balance between the reduction of horizontal stress due to unloading and the increase of horizontal stress due to the movement of the wall into the excavation (depending on relative flexibility of the wall and type of support). As shown in Fig. 16, the effective stress path may correspond to an increase or a decrease of horizontal effective stress.

For the soil behind the wall, there is a reversal in the direction of the stress path between concreting and main excavation. This should result in a stiff response during excavation, with the rapid mobilisation of active strength with shear strain. For a soil element in front of the wall, the change in the direction of the stress path between concreting and excavation is smaller and its response should be significantly less stiff.

To evaluate the response of the hypoplastic model, a series of numerical single element triaxial tests were

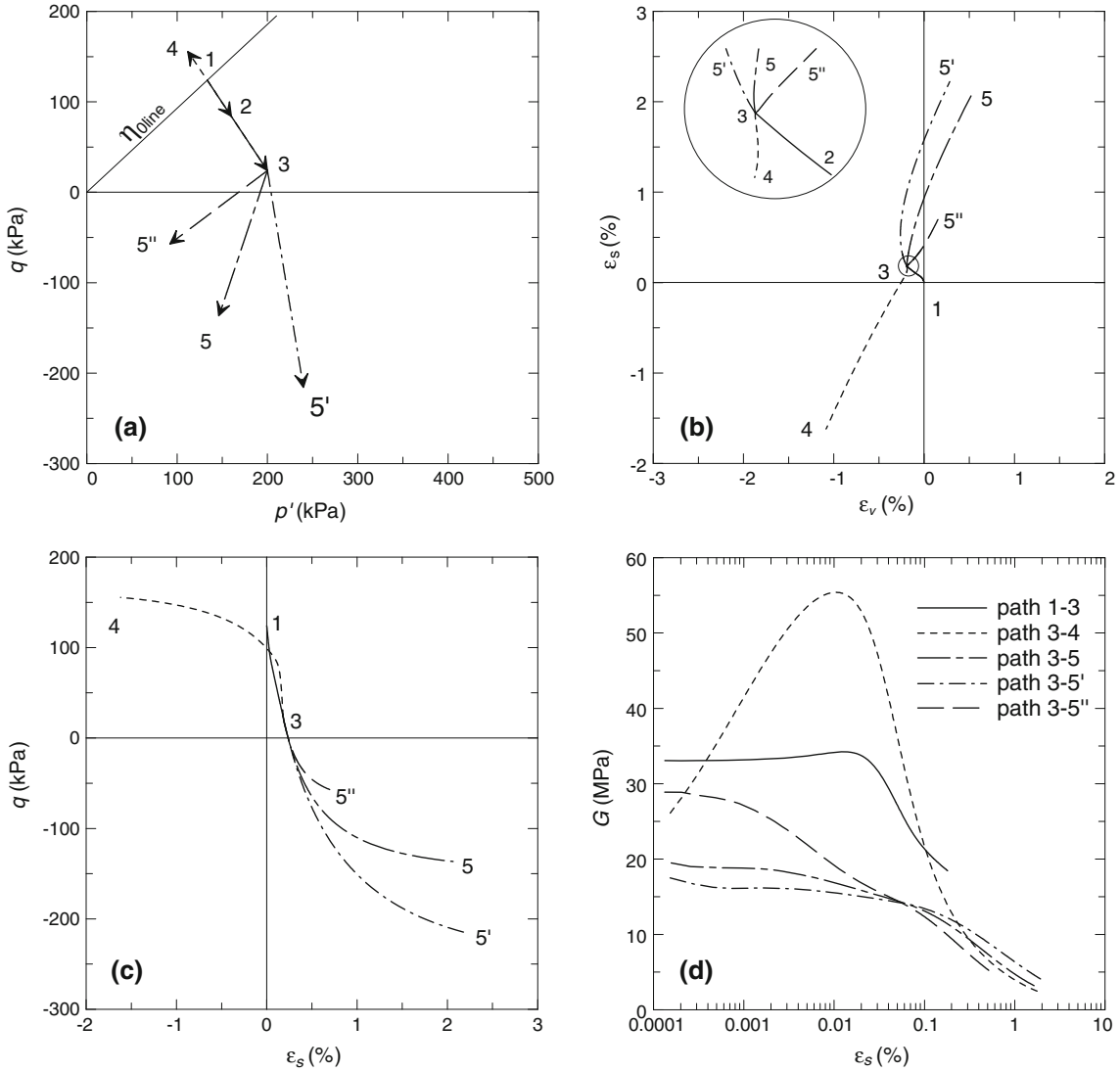

Fig. 17 **a** Stress paths followed by soil elements in TX tests in p':q space, **b** computed strain paths, **c** stress strain curves and **d** mobilised shear stiffness

carried out following the stress paths reported in Fig. 17a in the p':q plane, characterised by stress reversals that are qualitatively similar to those shown in Fig. 16. Although the deformation in the field occurs at least approximately in plane strain, whereas the deformation in the triaxial test is radially symmetric, it was considered that this would not mask the effect of the recent stress history of the soil; the differences of behaviour obtained for different stress paths are much larger than the variation in soil stiffness resulting from the kinematic difference between triaxial and plane strain compression and extension [31].

All triaxial stress paths start from the in situ stress at a depth of 12 m below ground level. After the common path (1–2–3), there is either a reduction of horizontal effective stress at constant vertical effective stress (3–4) or a reduction in vertical effective stress; following Powrie et al. [31], this was accompanied by no changes of horizontal effective stress, $\Delta\sigma'_h = 0$ (3–5), or an increase of the horizontal effective stress, $\Delta\sigma'_h = -\Delta\sigma'_v$ (3–5′) or a decrease of horizontal effective stress, $\Delta\sigma'_h = 1/2\Delta\sigma'_v$ (3–5″). The corresponding computed strain paths, in the ε_v:ε_s plane, deviatoric stress versus shear strain curves, and mobilised secant stiffness versus shear strain amplitude, are given in Fig. 17b, c and d, respectively. The operative mobilised secant stiffness along each path was defined as $G_{sec} = (q - q_0)/3(\varepsilon_s - \varepsilon_{s0})$, where q_0 and ε_{s0} are the values of deviatoric stress and deviatoric strain at the beginning of the stress path.

For stress paths 3–5, 3–5′ and 3–5″, the computed strain paths rotate clockwise relative to the strain path corresponding to the previous common stage (1–2–3) and the soil dilates to failure. The largest change of direction of the

strain path occurs for stress path 3–5″, and, accordingly, the initial mobilised stiffness is the highest. For stress path 3–5′, the computed strain path continues with nearly the same direction as the strain path corresponding to the previous stage; consequently, the stiffness of the soil continues to decrease from approximately the same value mobilised at the end of the common stage. For stress path 3–4, a counter clockwise change of direction of the strain path occurs and the soil contracts to failure. The initial increase of stiffness is of the same order as that obtained for stress path 3–5″ but, as the soil contracts, the stiffness continues to increase with straining until it reaches a value that is larger than the original stiffness of the in situ soil. Eventually, on continued straining with nearly the same direction, the stiffness decreases. As expected, at shear strains of the order of 10^{-2}%, the soil experiencing a complete reversal in the direction of the stress path between the common loading stage and the subsequent loading stage exhibits the stiffer response.

As the behaviour of the Mohr–Coulomb model before failure is linearly elastic, the mobilised stiffness along all paths is the same, and the model is unable to capture neither the high small-strain stiffness on stress reversal nor the effects of the recent history on the mechanical response.

Figure 18a shows the stress paths computed in the WIM 2D finite element analyses carried out with the hypoplastic model at positions A, A′, B and B′, located 12 m below ground surface at different distances from the wall, on the excavated and on the retained side of the wall. During wall installation, the horizontal stress at all positions increases to a value, which is very close to the lateral pressure applied by bentonite and wet concrete for the soil elements closer to the trench, and slightly smaller than this value at a larger distance from the wall. However, stress redistribution causes the vertical stress to change from its in situ value; these changes are larger for the soil elements that are closer to the trench. The stress paths during excavation are qualitatively similar to those adopted for the single element tests, although for soil elements on the retained side, the shear stress due to friction at the contact between the soil and the wall causes the vertical stress to decrease as the stress state moves towards active failure. The stress paths followed by soil elements in front of the wall closely match path 3–5″.

During excavation, the Mohr–Coulomb model overpredicts ground heave around the excavation; for a perfect contact between the wall and the soil, this induces large shear stresses in the soil around the wall. For soil elements on the retained side this produces unrealistic increments of vertical effective stress; closer to the wall the stress state moves towards passive failure with hardly any change in vertical effective stress. Therefore, the analyses carried out with the Mohr–Coulomb model were repeated inserting in the mesh a layer of interface elements with a thickness of 0.2 m at the contact between the wall and the soil, with reduced strength parameters ($c' = 2$ kPa and $\varphi' = 20°$). The stress paths computed using the Mohr–Coulomb model and interface elements are shown in Fig. 18b. For soil elements in front of the wall, they resemble paths 3–5 or 3–5′, depending on the position of the soil element relative to the wall. The differences with the hypoplastic predictions are likely to be still an effect of the shear stresses induced in the soil mass due to excessive heave.

4.2 Results

Figures 19 and 20 show the profiles of horizontal displacements of the wall and vertical displacements of the ground surface for $h = 5$ m and $h = 10$ m, respectively. In

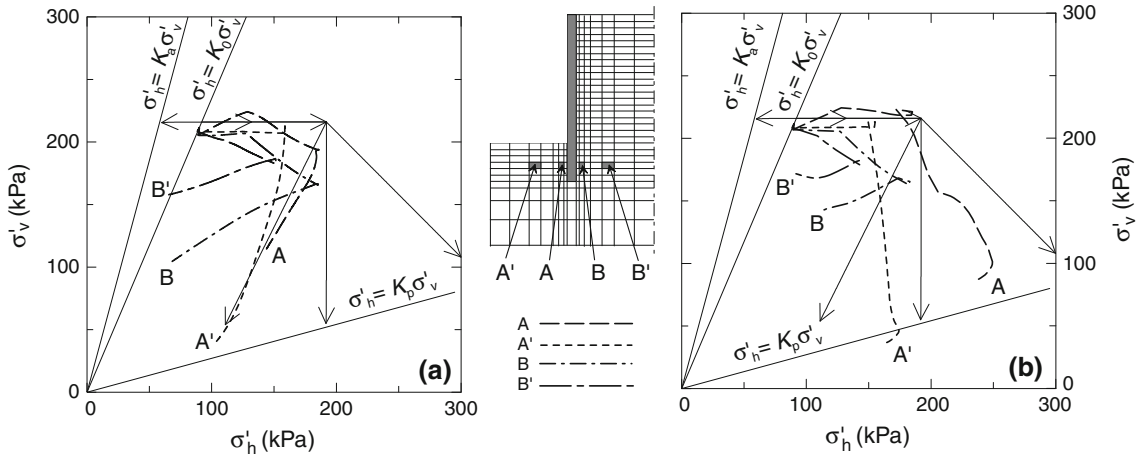

Fig. 18 WIM 2D analyses. Computed stress paths for soil elements behind and in front of the retaining wall: **a** hypoplastic and **b** Mohr–Coulomb model with interfaces

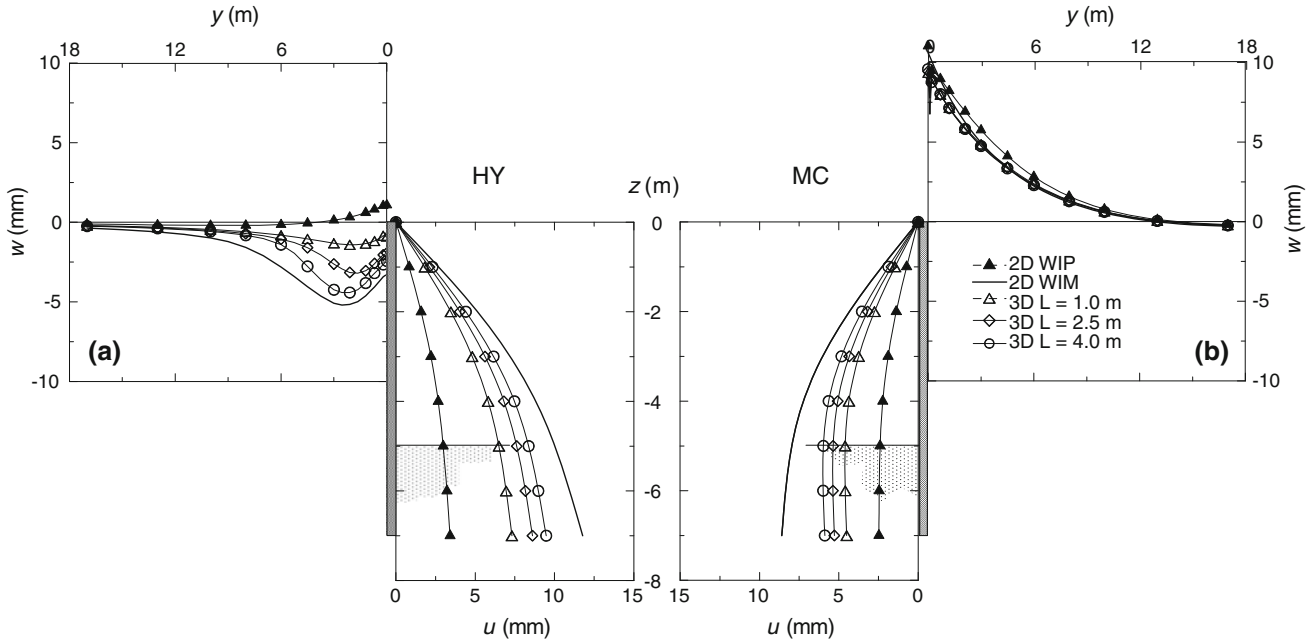

Fig. 19 $h = 5$ m. Computed horizontal displacements of the wall and vertical displacements of the ground surface: **a** hypoplastic and **b** Mohr–Coulomb model

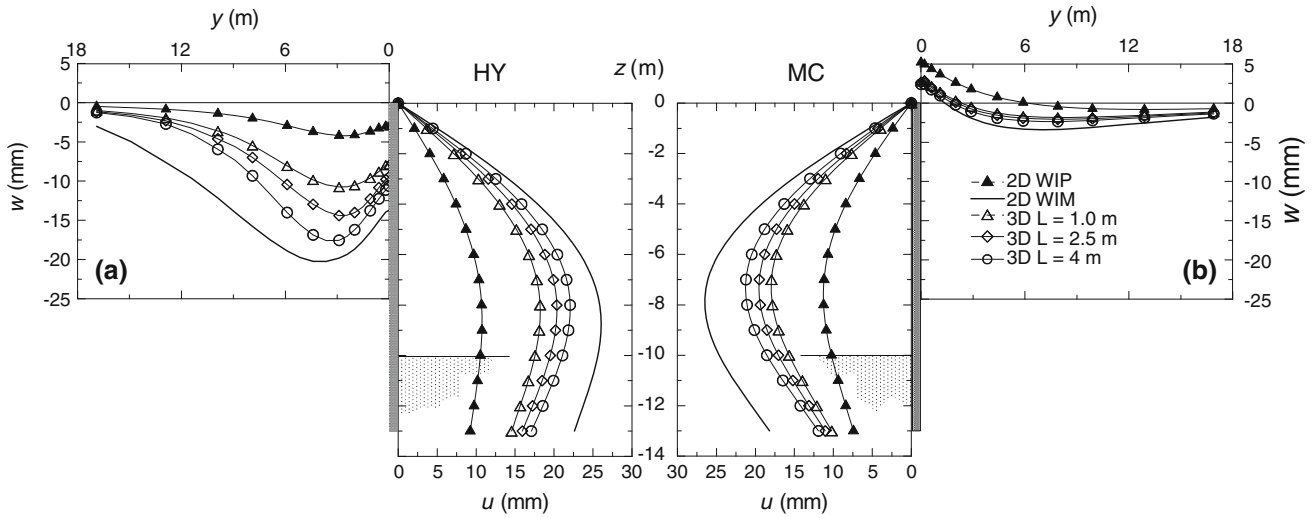

Fig. 20 $h = 10$ m. Computed horizontal displacements of the wall and vertical displacements of the ground surface: **a** hypoplastic and **b** Mohr–Coulomb model

order to have a direct comparison with the experimental observations, increments of displacements relative to the end of the installation stage are reported. The displacements computed at the centre of the primary and secondary panel are the same.

Panel length has a significant effect on the magnitude of the computed horizontal displacements of the wall. WIM 2D analyses model wall installation as the excavation of an infinitely long slot, and therefore they overestimate installation effects and provide one bound of the results; the other bound is represented by the results of the WIP analyses. As the length of the panels increases, the results move closer to those obtained by WIM 2D analyses but the predicted deflected shape of the wall is hardly affected by panel length.

Three-dimensional hypoplastic analyses (Figs. 19a, 20a) predict settlements of the ground surface behind the wall that extend to a maximum distance from the wall between $1.5 \times h$ and $2 \times h$. As for the horizontal displacements, panel length has a significant effect on the magnitude of the

vertical displacements and the results are bounded by those obtained modelling installation in plane strain and those obtained for a WIP wall. Only for the 5 m high wall, WIP analyses predicted a small heave close to the wall. The extent of the surface settlement trough predicted by plane strain analyses, both WIM 2D and WIP, is slightly larger than that predicted by three-dimensional analyses.

The horizontal displacements obtained using the Mohr–Coulomb model (Figs. 19b, 20b) are similar to those obtained for the hypoplastic model, both in magnitude and deflected shape of the wall; however, the horizontal displacements of the toe of the wall predicted by the hypoplastic model are slightly larger than those predicted using the Mohr–Coulomb model, probably due to the lower stiffness of the soil elements in front of the wall. The profile of surface displacements predicted by the Mohr–Coulomb model is not realistic, with substantial heave behind the wall. Also, for both depths of excavation, the effect of panel length on the predicted vertical displacements of the ground surface is less pronounced than for hypoplastic analyses.

Figure 21 shows the profiles of vertical displacements at ground surface computed in the finite element analyses and some experimental observations for excavations in sand [5]. The results obtained using the hypoplastic model and modelling wall installation are consistent with the available observations, both in magnitude and trend while, if installation of the wall is not modelled, computed ground settlements behind the wall are substantially smaller than observed, even using the more complex non-linear model. This is consistent with previous studies of the effects of using non-linear constitutive models on the predicted vertical displacements behind excavations [13, 43]. On the other hand, the analyses carried out using the Mohr–Coulomb model, both modelling wall installation or wishing the wall in place, yield unrealistic values of surface heave.

Figures 22 and 23 show the bending moments computed at the centre of the primary panel using the two constitutive

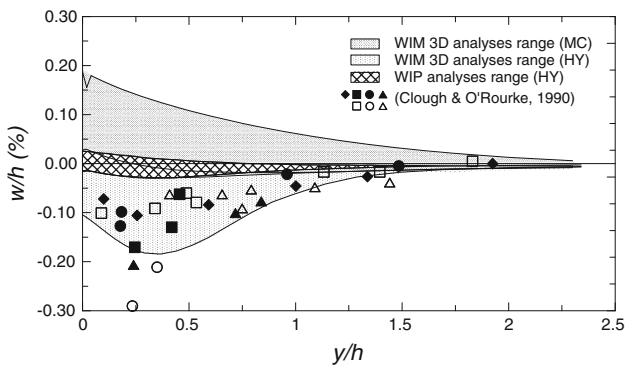

Fig. 21 Comparison of computed vertical displacements of ground surface due to excavation with data reported in the literature

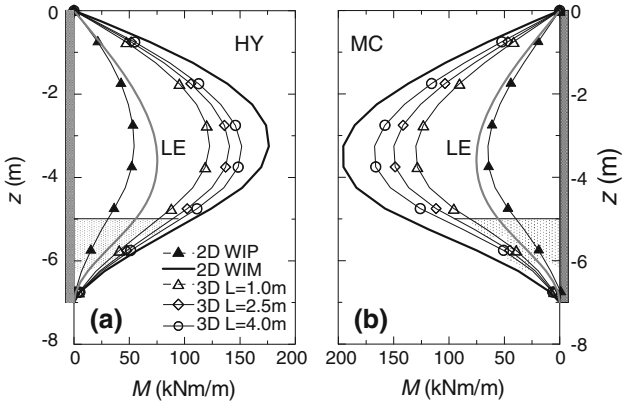

Fig. 22 $h = 5$ m. Computed bending moments in the wall: **a** hypoplastic and **b** Mohr–Coulomb model

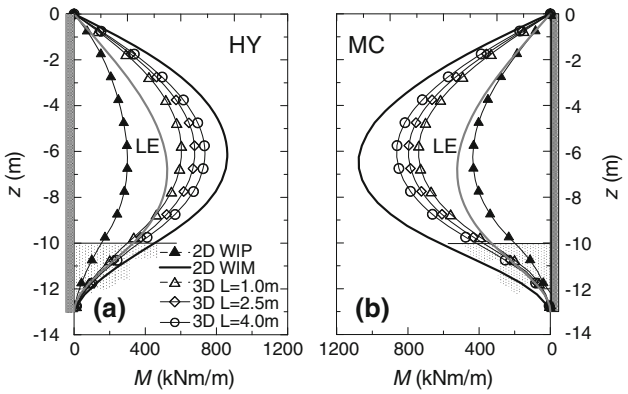

Fig. 23 $h = 10$ m. Computed bending moments in the wall: **a** hypoplastic and **b** Mohr–Coulomb model

models, for $h = 5$ m and $h = 10$ m, respectively, while the corresponding values of prop forces are summarised in Table 2. The bending moments computed at the centre of the secondary panel are only slightly larger than those shown in the figures (by about 5%), notwithstanding the fact that at the end of installation, the earth pressures behind the secondary panel were significantly larger than those at the back of the primary panel (see Fig. 6). This is due to the redistribution of stress on excavation caused by the wall stiffness. Panel length affects significantly the results that are bounded by those obtained from WIM 2D and WIP analyses, both in terms of bending moments and prop forces. The bending moments computed using the Mohr–Coulomb model are slightly larger than those computed using the hypoplastic model, and the maximum value of the bending moment occurs at a slightly deeper position on the wall. The overall picture, however, is not significantly different from that obtained with the hypoplastic model.

The bending moments and the prop forces were also computed by limit equilibrium (LE), assuming that the active limit state is always attained in the soil on the

Table 2 Computed prop forces in kN/m

h (m)	Constitutive model	WIP	WIM 3D $L = 1$ m	WIM 3D $L = 2.5$ m	WIM 3D $L = 4$ m	WIM 2D	LE
10	HY	112	191	204	208	303	115
	MC	114	215	231	241	390	
5	HY	36	72	76	78	114	31
	MC	25	58	64	68	118	

retained side of the wall and that a constant proportion of the passive effective strength, found considering the equilibrium of moments about the prop, is mobilised along the entire embedded length. This is consistent with combination C1 of partial factors of Design Approach DA1 of Eurocode 7 [11] and of the new Italian technical code [28], in which soil parameters are not factored when the structural safety has to be evaluated, while the loads or their effects are amplified using factors larger than one. As both codes do not permit the use of partial factors on the soil unit weight, in the absence of external loads, the use of DA1-C1 to evaluate the internal forces in a retaining wall consists essentially in performing the calculations using characteristic values of all the parameters together with a credible estimate of the distribution of contact stress, that is, at least respectful of equilibrium equations. Structural safety may then be evaluated applying partial factors of combination C1 to the effects of the loads, such as bending moments and prop forces [4, 12].

The bending moments and the prop forces computed by LE are also shown in Figs. 22 and 23 and included in Table 2 for comparison. The bending moments computed by LE are larger than those computed from WIP analyses but always smaller than those computed from WIM analyses for all panel lengths. This can be explained by the distribution of horizontal stresses acting on the wall at the end of excavation. Figures 24 and 25 show the computed distribution of the horizontal stress at the centre of the primary panel using the two constitutive models for $h = 5$ m and $h = 10$ m, respectively. The magnitude of the horizontal stresses at the centre of the secondary panel is different from that at the centre of the primary panel by an amount that depends on panel length, but the trend of the contact stresses for the different analyses is the same. Also included in the figures are the theoretical active and passive stresses and the distribution of reduced passive stress adopted along the embedded length for the LE calculations. For the WIM 2D analyses, the stress acting on the retained side of the wall at the end of excavation is still much larger than that corresponding to the active limit state, as wall displacements are not sufficient to reduce the large initial stresses computed at the end of installation. On the other hand, if the wall is WIP, the horizontal stresses acting on the retained side of the wall at the end of excavation are very close to the active value, but for the upper part of the wall where the prop prevents horizontal movements. A similar trend can be observed on the passive side, where the final horizontal stresses computed at the end of excavation for WIM 2D analyses are much larger than those computed for a WIP wall. The distribution of horizontal stress adopted in the LE calculations is very close to that obtained for WIP analyses on the retained side of the wall; however, the horizontal stresses in front of the wall are substantially different from those obtained at the end of WIP analyses, and this affects the computed values of bending moment. Panel length affects significantly the final distribution of horizontal stress computed on both sides of the wall, and the horizontal stresses obtained from WIM 3D analyses are bounded by those obtained from WIM 2D and WIP analyses.

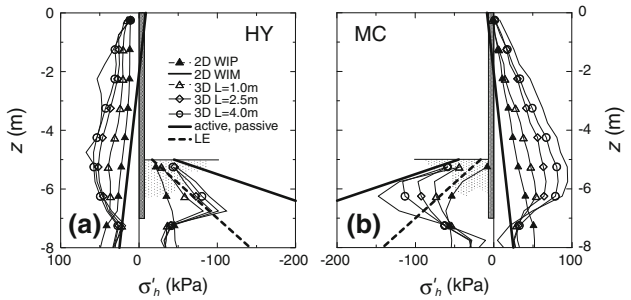

Fig. 24 $h = 5$ m, Centre of *primary panel*. Computed distribution of horizontal stresses along the wall: **a** hypoplastic and **b** Mohr–Coulomb model

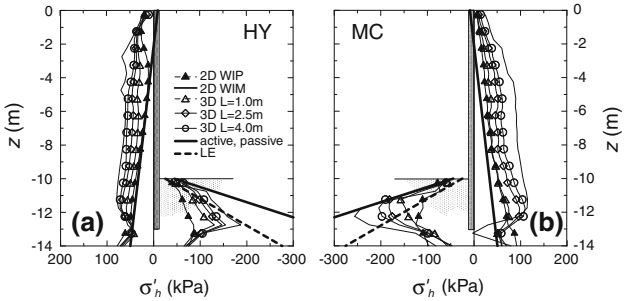

Fig. 25 $h = 10$ m, Centre of *primary panel*. Computed distribution of horizontal stresses along the wall: **a** hypoplastic and **b** Mohr–Coulomb model

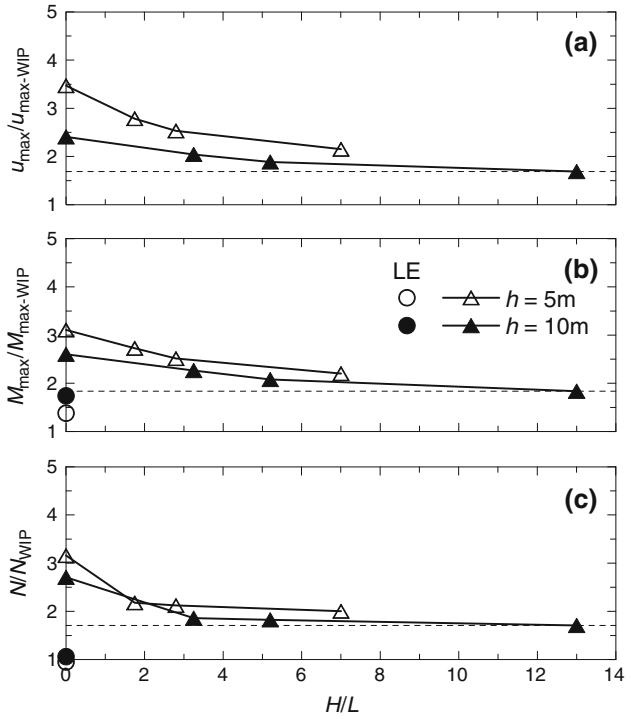

Fig. 26 **a** Maximum horizontal displacements, **b** maximum bending moments and **c** axial prop forces normalised by the corresponding quantity obtained from WIP analyses as a function of panel aspect ratio, *H*/*L*

Figure 26a shows the maximum computed horizontal displacements of the wall, normalised by the corresponding displacement obtained from WIP analyses, as a function of *H*/*L*. As the panel aspect ratio, *H*/*L*, is reduced the maximum displacement increases towards the value computed with WIM 2D analyses ($L \rightarrow \infty$), at an accelerating rate. The normalised displacement at $H/L = 0$ is between 3 and 4, depending on wall height. A lower bound of about 1.7, shown as a horizontal dashed line in Fig. 26a, can be easily identified at large values of *H*/*L*, corresponding to the installation of an infinity of panels of zero length. The data indicate that a prediction carried out wishing the wall in place underestimates the maximum wall deflections for all panel lengths. The lower bound of 1.7 can be considered a sort of intrinsic amplification caused by installation that is not susceptible of further reduction.

Figure 26b, c show the maximum computed bending moments and axial forces in the prop, normalised by the corresponding quantity obtained from WIP analyses, as a function of *H*/*L*, for both $H = 7$ m and $H = 13$ m. The maximum structural loads computed from WIM 2D analyses are about 3 times those computed from WIP analyses, independently of wall height; lower bounds of about 1.8 and 1.7 are obtained at large values of *H*/*L*, again shown as horizontal dashed lines in the corresponding figures. A prediction carried out wishing the wall in place underestimates the maximum bending moments and prop forces for all panel lengths.

5 Conclusions

For underground construction in urban environment, one of the main design requirements is that of limiting ground deformations caused by the changes of stress due to excavation. Ground movements, including those associated with retaining structure installation, must therefore be predicted with reasonable accuracy. Displacements associated with excavations may be estimated based on experimental observations or their magnitude predicted by numerical analyses. Ideally, these should be three-dimensional analyses, as stress transfer and ground deformation during wall installation and subsequent excavation are strongly three-dimensional phenomena, and should be carried out using a constitutive model capable to reproduce the main features of soil behaviour, such as irreversibility, non-linearity and stress-history dependence even at small strains.

With reference to the installation stage, the results of our study indicate that the horizontal displacements due to diaphragm wall installation computed numerically in plane strain analyses may be corrected using curves similar to those in Fig. 13 to take into account their reduction with panel aspect ratio. However, other factors may affect the results, such as, for example, soil properties, initial conditions, presence of a pore water pressure in the field and soil/water interaction, and further parametric studies would be required to define the shape of a general "correction curve". The results of two-dimensional numerical analyses carried out using a simple constitutive model, such as Mohr–Coulomb, depend critically on the adopted value of the elastic stiffness. As the shear strain levels during the installation stage are much smaller than those mobilised during the main excavation, realistic predictions of horizontal ground movements with linear elastic perfectly plastic models can only be obtained using a value of stiffness larger than that used to predict behaviour in the subsequent excavation stage.

The results of our study indicate that only three-dimensional analyses carried out with advanced constitutive models predict surface settlements during wall installation; two-dimensional analyses, even if carried out with advanced constitutive models, predict surface heave behind the wall. Two- and three-dimensional numerical analyses carried out using the Mohr–Coulomb constitutive model always predict substantial and unrealistic surface heave behind the wall, even adopting relatively high values of stiffness.

Numerical analyses of the main excavation stage is generally carried out ignoring wall installation, that is, the

wall is WIP at the beginning of the analyses. However, wall installation has a significant effect on the subsequent behaviour of the retaining structure as it modifies the lateral stresses behind the wall and the recent stress history of the soil. Three-dimensional analyses carried out with advanced constitutive models and in which wall installation is explicitly modelled predict surface settlements behind the wall consistent with the experimental observations both in magnitude and trend. A comparison of the results obtained from analyses in which wall installation is modelled and those where the wall is WIP, shows that it is not sufficient to have a highly non-linear constitutive model to predict correctly ground movements and structural loads if the initial stress state and the recent stress history are not included in the analyses.

The results of this work also show that the maximum horizontal wall deflections, bending moments and prop forces reduce with increasing panel aspect ratio, H/L, towards a minimum value, which is about twice the corresponding value computed for WIP analyses. Decreasing panel length reduces the amplification of wall deflections and structural loads up to a panel aspect ratio of about 3; no further improvement is obtained for larger panel aspect ratios. Bending moments computed using LE, widely adopted at the preliminary design stage, are always smaller than those obtained by modelling installation.

For any given aspect ratio, the horizontal wall deflections and structural loads due to excavation can be successfully back analysed also with plane strain analyses in which wall installation is not modelled and simple constitutive models are used with appropriate selection of soil stiffness [9]. On the contrary, the pattern and magnitude of surface vertical displacements are much more influenced than wall deflections by non-linear soil behaviour, and therefore, the results obtained from linearly elastic-perfectly plastic analyses, no matter whether 3D or 2D, are generally unrealistic.

Acknowledgments The work described in this paper was prompted by the construction of some of the new stations of Napoli Underground; the Authors wish to express their gratitude to Alessandro Mandolini for creating the opportunity to work together, for his many valuable comments, energy and general support. The routine for the extended hypoplastic model was provided by Ivo Herle while precious advise on the numerical modelling was given by Claudio Tamagnini.

References

1. Al-Tabbaa A, Wood DM (1989) An experimental based 'bubble' model for clay. In: Proceedings of 3rd international conference on numerical models in geomechanics, Niagara Falls, pp 91–99
2. Atkinson JH, Coop MR, Stallebrass SE, Viggiani G (1993) Measurement of stiffness of soils and weak rocks in laboratory tests. In: Proceedings of 25th annual conference Engineering Group of the Geological Society, Leeds, pp 21–27
3. Burland JB, Hancock RJR (1977) Underground car park at the House of Commons: geotechnical aspects. Struct Eng 55:87–100
4. Callisto L (2010) A factored strength approach for the limit states design of geotechnical structures. Can Geotech J 47(9):1011–1023
5. Clough GW, O'Rourke TD (1990) Construction induced movements of in situ walls. In: PC Lambe, LA Hansen (eds) Design and performance of earth retaining structures. ASCE GSP No. 25, Ithaca, pp 430–470
6. Dafalias YF (1986) Bounding surface plasticity. I: mathematical foundation and hypoplasticity. J Eng Mech ASCE 112(9):966–987
7. Dafalias YF, Herrmann LR (1986) Bounding surface plasticity. II: application to isotropic cohesive soils. J Eng Mech ASCE 112(12):1263–1291
8. De Moor EK (1994) An analysis of bored pile/diaphragm wall installation effects. Géotechnique 44(2):341–347
9. De Sanctis L, Mandolini A, Viggiani GMB (2006) Finite element analysis of the excavation of the new Garibaldi station of Napoli underground. In: Triantafyllidis T (ed) Numerical modelling of construction processes in geotechnical engineering for the urban environment. Bochum, Taylor & Francis, London, pp 57–68
10. de Wit JCWM, Lengkeek HJ (2002) Full scale test on environmental impact of diaphragm wall trench installation in Amsterdam. In: Proceedings of international symposium on geotechnical aspect of underground construction in soft ground, Toulose, France
11. EN (1997) Eurocode 7, part I: geotechnical design—general rules
12. Frank R, Bauduin C, Driscoll R, Kavvadas M, Krebs Ovesen N, Orr T, Schuppener B (2004) Designers' guide to EN 1997–1: Eurocode 7: geotechnical design—general rules. Thomas Telford, London
13. Finno RJ, Harahap IS, Sabatini PJ (1991) Analysis of braced excavations with coupled finite element formulations. Comput Geotech 2:91–114
14. Gourvenec SM, Powrie W (1999) 3D finite-element analysis of diaphragm wall installation. Géotechnique 49(6):801–823
15. Gunn MJ, Clayton CRI (1992) Installation effects and their importance in the design of earth retaining structures. Géotechnique 42(1):137–141
16. Gunn MJ, Satkunananthan A, Clayton CRI (1992) Finite element modelling of installation effects. Proc ICE Retain Struct 46–55
17. Herle I, Gudehus G (1999) Determination of parameters of a hypoplastic constitutive model from properties of grain assemblies. Mech Cohes Frict Mater 4:461–486
18. Jardine RJ, Potts DM, Fourie AB, Burland JB (1986) Studies on the influence of non-linear stress–strain characteristics in soil–structure interaction. Géotechnique 36(3):377–396
19. Kolymbas D (1991) An outline of hypoplasticity. Arch Appl Mech 61:143–151
20. Lächler A, Neher HP, Gebeyehu G (2006) A comparison between monitoring data and numerical calculation of a diaphragm wall construction in Rotterdam. In: Triantafyllidis T (ed) Numerical modelling of construction processes in geotechnical engineering for the urban environment. Bochum, Taylor & Francis, London, pp 83–96
21. Lings ML, Nash DFT, Ng CWW, Boyce MD (1991) Observed behaviour of a deep excavation in Gault clay: a preliminary appraisal. In: Proceedings of tenth European conference on soil mechanics and foundation engineering, Florence, vol 2, pp 467–470
22. Lings ML, Ng CWW, Nash DFT (1994) The lateral pressure of wet concrete in diaphragm wall panels cast under bentonite. Proc Inst Civ Eng Geotech Eng 107:163–172
23. Mayer PM, Gudehus G (2002) Prediction of soil movements due to diaphragm wall construction. Geotech Spec Publ 116:696–712
24. Ng CWW (1994) Effects of modelling wall installation on multi-staged excavations in stiff clays. In: Proceedings 1st international

conference on 'pre-failure deformation of geomaterials', Sapporo vol 1, pp 595–600
25. Ng CWW, Lings ML, Simpson B, Nash DFT (1995) An approximate analysis of the three dimensional effects of diaphragm wall installation. Géotechnique 45(3):497–507
26. Ng CWW, Yan RWM (1998) Stress transfer and deformation mechanisms around a diaphragm wall panel. J Geotech Geoenviron Eng Div ASCE 124(7):638–648
27. Niemunis A, Herle I (1997) Hypoplastic model for cohesionless soils with elastic strain range. Mech Cohes Frict Mater 2:279–299
28. NTC (2008) Nuove Norme Tecniche per le Costruzioni. Gazzetta Ufficiale della Repubblica Italiana, No. 29, 4 Febbraio 2008—Suppl. Ordinario No. 30 (in Italian)
29. Pastor M, Zienkiewicz OC, Chan AHC (1990) Generalized plasticity and the modelling of soil behaviour. Int J Numer Anal Methods Geomech 14:151–190
30. Poh TY, Goh ATC, Wong IH (2001) Ground movements associated with wall construction: case histories. J Geotech Geoenviron Eng ASCE 127(12):1061–1069
31. Powrie W, Pantelidou H, Stallebrass SE (1998) Soil stiffness in stress paths relevant to diaphragm walls in clay. Géotechnique 48(4):483–494
32. Potts DM, Fourie AB (1884) The behaviour of a propped retaining wall: results of a numerical experiment. Géotechnique 34(3):383–404
33. Potts DM, Zdravković L (1999) Finite element analysis in geotechnical engineering: theory. Finite element analysis in geotechnical engineering. Thomas Telford, London
34. Rampello S, Stallebrass SE, Viggiani GMB (1998) Ground movements associated with excavations in stiff clays: current prediction capability. In: Proceedings of the 2nd international symposium on the geotechnics of hard-soils/soft rocks. Naples, vol 3, pp 1527–1540
35. Richards DJ, Powrie W, Page JRT (1998) Investigation of retaining wall installation and performance using centrifuge modelling techniques. Proc ICE Geotech Eng 131(3):163–170
36. Shäfer N, Triantafyllidis T (2004) Modelling of earth and water pressure development during diaphragm wall construction in soft clay. Int J Numer Anal Methods Geomech 28:1305–1326
37. Shäfer N, Triantafyllidis T (2006) The influence of the construction process on the deformation behaviour of diaphragm walls in soft clayey ground. Int J Numer Anal Methods Geomech 30(7):563–576
38. St. John HD, Potts DM, Jardine RJ, Higgins KG (1993) Prediction and performance of ground response due to construction of a deep basement at 60 Victoria Embankment. In: Houlsby GT, Schofield AN (eds) Proceedings of the Wroth memorial symposium on 'predictive soil mechanics'. Thomas Telford, London, pp 581–608
39. Stallebrass SE, Taylor RN (1997) The development and evaluation of a constitutive model for the prediction of ground movements in overconsolidated clay. Géotechnique 47(2):235–253
40. Symons IF, Carder DR (1993) Stress changes in stiff clay caused by the installation of embedded retaining walls. In: Clayton GC (ed) Retaining structures. Thomas Telford, London, pp 227–236
41. Tedd P, Chard BM, Charles JA, Symons IF (1984) Behaviour of a propped embedded retaining wall in stiff clay at Bell Common Tunnel. Géotechnique 34(4):513–532
42. Viggiani GMB, Mandolini A, Flora A, Russo G (2010) Excavations in the urban environment: examples from the construction of Napoli underground. Invited lecture. In: Proceedings of the international geotechnical conference on "geotechnical challenges in megacities", GeoMos2010, Moscow, 7–10 June 2010, vol 1, pp 236–258
43. Viggiani G, Tamagnini C (2000) Ground movements around excavations in granular soils: a few remarks on the influence of the constitutive assumptions on FE predictions. Mech Cohes Frict Mater 5:399–423
44. von Wolffersdorff PA (1996) A hypoplastic relation for granular materials with a predefined limit state surface. Mech Cohes Frict Mater 1:251–271